Journal of The Electrochemical Society, **166** (4) A464-A472 (2019)
0013-4651/2019/166(4)/A464/9/$38.00 © The Electrochemical Society

Transport and Electron Transfer Kinetics of Polyoxovanadate-Alkoxide Clusters

Anjula M. Kosswattaarachchi,[1,*] Lauren E. VanGelder,[2] Olaf Nachtigall,[2,3] Joshua P. Hazelnis,[1] William W. Brennessel,[2] Ellen M. Matson,[2,z] and Timothy R. Cook[1,z]

[1]*Department of Chemistry, University at Buffalo, State University of New York, Buffalo, New York 14260, USA*
[2]*Department of Chemistry, University of Rochester, Rochester, New York 14627, USA*
[3]*Institut für Chemie und Biochemie, Freie Universität Berlin, 14195 Berlin, Germany*

A family of four polyoxovanadate-alkoxide (POV-alkoxide) clusters was prepared and electrochemical techniques were used to evaluate diffusion coefficients and electron transport across a range of oxidation states. Synthetic routes were developed to increase the alkyl chain length of the $[V_6O_7(OR)_{12}]$ cores, increasing R from the previously reported R = CH_3, C_2H_5 to R = C_3H_7, C_4H_9. Whereas increasing chain length may enhance solubility, such modifications may also hinder diffusion and electron transfer by shielding the core, thus we experimentally determined these parameters using both cyclic voltammetry and rotating disk voltammetry. Increasing the alkyl chain length of the POV-alkoxide nanostructures from methoxide to butoxide changes the solubility from 0.205 to 0.297 M in acetonitrile. Although some variations in diffusion coefficients and heterogeneous electron transfer rate constants were observed across the suite of oxidation states from species to species, they range from 0.14×10^{-5} cm^2/s to 2.24×10^{-5} cm^2/s for D_0 and 0.56×10^{-3} cm/s to 209.00×10^{-3} cm/s for k_{het}. An increased chain length did not result in lower diffusion coefficients. Thus, we conclude that between C1 and C4 chains, no shielding of the redox core occurs, nor is transport through solution systematically hindered.
 [DOI: 10.1149/2.1351902jes]

Manuscript submitted November 27, 2018; revised manuscript received January 24, 2019. Published February 8, 2019.

Redox flow batteries (RFBs) are an important electrochemical energy storage (EES) technology due to their independent scalability of energy and power.[1] A myriad of redox-active molecules have been explored as charge-carriers in RFBs and significant efforts have been made to identify highly soluble charge-carriers that have long-term stability, motivated by the terms contributing to the volumetric energy density (E_{vol}) of a RFB device:

$$E_{vol} = \frac{1}{2} n V_{cell} F C_{active} \quad [1]$$

Where n is the number of electrons transferred, V_{cell} is the average cell voltage, F is Faraday's constant, and C_{active} is the concentration of the charge carrier. Non-aqueous RFBs (naRFBs) allow exploitation of the properties of organic solvents, which include both wide redox windows and operating temperatures.[2] Although there are a number of organic solvents that do not interfere with the charge/discharge of active species, many are impractical for actual RFB devices. Beyond redox windows, cost, mass-transport properties, and membrane compatibilities are all practical factors to be considered.[3,4] Darling, Gallagher, Brushett and co-workers have done a comprehensive cost analysis for naRFBS[4] and also studied transport characteristics including area specific resistance (ASR), cross-over current density, and coupling between crossover and capacity loss toward establishing a general quantification strategy for solvents and membrane separators.[3] DMF and DMSO were recognized as highly conducting solvents that can be used in tandem with Nafion 211 to achieve an ASR target of 2.3 Ω cm^2. Yan and co-workers identified acetonitrile as another good solvent for naRFBs, due to its low viscosity and high ionic conductivity.[5]

A large collection of coordination complexes,[6–11] organic compounds,[12–18] and redox active polymers[19–21] have been explored as components of naRFBs; however, the widespread commercialization of naRFB technologies remains limited due to high capital cost, low power and energy density, and relatively rapid capacity fade over long-term cycling—all factors that are critically linked to the physical and electrochemical properties of charge-carriers.[1,22] To date, there remains a lack of suitable redox active molecules with the necessary physicochemical properties to address the aforementioned challenges facing improvements of existing naRFB technologies.

To enhance the viability of naRFB technologies, charge carriers must be designed to feature (1) kinetically fast and chemically reversible redox reactions; (2) multiple reversible redox events over a large electrochemical window; (3) high chemical, electrochemical, and cell-component stability across all operative oxidation states; (4) high solubility in organic solvents; and (5) composition from inexpensive, earth-abundant starting materials. Nanoscopic polynuclear architectures are excellent candidates as high-energy capacity naRFB active species, as they can be systematically modified to obtain multi-electron transfer and long-term stability, while simultaneously addressing membrane crossover, solubility, and redox potential.[23] However, there remains a poor understanding of approaches for the derivation of new classes of polynuclear assemblies with fundamental properties relevant for EES, particularly in nonaqueous media. Filling this gap in knowledge requires comprehension of the structure-function relationships that inform how size, nuclearity, ligand design, and metal composition control the electrochemical and physicochemical profiles of multimetallic charge carriers. Whereas pioneering work on small organic molecules and coordination complexes reveals the power of leveraging molecular-level knowledge and design,[24–28] to date such a systematic approach is underdeveloped for polynuclear assemblies.

We have recently identified and characterized a series of discrete, self-assembled polyoxovanadate-alkoxide (POV-alkoxide) clusters, $[V_6O_7(OR)_{12}]$, as suitable charge-carriers for naRFBs.[23,29,30] In our initial work, it was demonstrated that the ligand modification at the bridging alkoxide moieties from a -CH_3 group to -C_2H_5 group results in significant improvement in cluster stability during charge–discharge cycling.[23] In addition, we note that the carbon number in the bridging alkyl groups has significant bearing on the overall solubility of the clusters. The results observed in our preliminary studies prompted the evaluation of homoleptic ligand substitution of POV-alkoxide clusters on the electrochemical and physicochemical behavior in solution, toward the ultimate goal of developing superior charge-carriers for naRFBs. In this work, we explore the electrochemical consequences of extending alkyl-chain length of the bridging alkoxide ligands, with a focus on the comparative electronic transfer kinetics of $[V_6O_7(OMe)_{12}]$ (**1**), $[V_6O_7(OEt)_{12}]$ (**2**), $[V_6O_7(O^nPr)_{12}]$ (**3**), and $[V_6O_7(O^nBu)_{12}]$ (**4**) POV-alkoxide clusters. Whereas increasing the chain length is attractive from the standpoint of increasing solubility, there have been no investigations on whether or not these changes hinder electron transfer in a systematic way. Therefore, we have measured the diffusion coefficients (D_0) of a suite of C1 to C4 alkoxide ligands and the various charge states of the ethoxide variant and the heterogeneous electron transfer rate constants (k_0) of all relevant redox couples. We used acetonitrile as the solvent in this study as it

*Electrochemical Society Student Member.
[z]E-mail: trcook@buffalo.edu; ellen.matson@rochester.edu

effectively solubilized the clusters at all-relevant oxidation states, enabling investigations of longer-term stability.[23]

D_0 and k_0 parameterize the mass transport and electron transfer properties of an electrochemical reaction that have ramifications on charge transfer resistance, and are therefore critically important for establishing the viability of a charge carrier.[31,32] The most common methods used for analyzing RFB charge carriers are rotating disk electrode voltammetry (RDE) and cyclic voltammetry (CV).[8,9,33] We report the values of D_0 obtained using the Randles-Sevcik method,[34] and estimated k_0 values using the Nicholson,[35] Kochi-Klinger,[36] and Koutecky-Levich methods.[37] In addition to the electrochemical kinetics and transport parameters, we present the impact of bridging-alkoxide ligand substitution on stability and solubility of the homoleptic POV-alkoxide clusters in acetonitrile. Together, these rigorous analyses establish chain-length independence of electron transfer, suggesting ligand modifications as an ideal way to improve the energy density of POV-alkoxide derived charge-carriers for non-aqueous electrochemical energy storage.

Experimental

Synthesis and characterization.—*General considerations.*—Manipulations which required the absence of water and oxygen were conducted in a UniLab MBraun inert atmosphere glove box under a dinitrogen atmosphere. Glassware was oven dried for a minimum of 4 hours and cooled in an evacuated antechamber prior to use in the glove box. Anhydrous methanol, ethanol, propanol, and butanol were purchased from Sigma-Aldrich and stored over activated 4 Å molecular sieves purchased from Fisher Scientific. All other solvents were dried and deoxygenated on a Glass Contour System (Pure Process Technology, LLC) and stored over activated 4 Å molecular sieves. V_2O_5 (99.5% approx., 60 mesh), [^{n}Bu$_4$N][BH$_4$], and VO(O^nPr)$_3$ were purchased from Sigma-Aldrich and used as received. [V_6O_7(OMe)$_{12}$] (**1**) and [V_6O_7(OEt)$_{12}$] (**2**) were prepared according to literature precedent.[23,38] TBAPF$_6$ was purchased from Sigma-Aldrich, recrystallized thrice using hot methanol, and stored under dynamic vacuum for a minimum of two days prior to use. ^{1}H NMR spectra were recorded on a Bruker DPX-500 spectrometer locked on the signal of deuterated solvents. All chemical shifts were reported relative to residual proteo solvent resonances. CD_3CN was purchased from Cambridge Isotope Laboratories, degassed by three freeze−pump−thaw cycles, and stored over activated 4 Å molecular sieves. Infrared (FT-IR, ATR) spectra of complexes were recorded on a Shimadzu IRAffinity-1 Fourier Transform Infrared Spectrophotometer and are reported in wavenumbers (cm^{-1}). Electronic absorption measurements were recorded at room temperature in anhydrous acetonitrile in a sealed 1 cm quartz cuvette with an Agilent Cary 60 UV-Vis spectrophotometer. Mass spectrometry analyses were performed on an Advion expression^L Compact Mass Spectrometer equipped with an electrospray probe and an ion-trap mass analyzer. Direct injection analysis was employed in all cases with a sample solution in acetonitrile. Single crystals were mounted on the tip of a thin glass optical fiber and positioned on a XtaLab Synergy-S Dualfelx diffractometer equipped with a HyPix-6000He HPC area detector for data collection at 100.0(5) K. The structures were solved using SHELXT-2014/5[39] and refined using SHELXL-2014/7.[40] Elemental analyses were performed on a PerkinElmer 2400 Series II Analyzer, at the CENTC Elemental Analysis Facility, University of Rochester.

Preparation of VO(O^nBu)$_3$.—The preparation of this mononuclear vanadium precursor is based on a modification of the previously published procedure.[41] A stirred suspension of V_2O_5 (70.0 g, 385 mmol) in 600 mL ^{n}BuOH was heated in a 1 L round bottom flask equipped with reflux condenser to 80–90°C under argon atmosphere overnight. Stirring was then turned off and the temperature of the system was reduced to 60°C. V_2O_5 was allowed to settle at the bottom of the flask for 30 min. The warm reaction mixture was gently decanted in portions of 100–150 mL into a fritted filter funnel. The flask was constantly flushed with argon during the filtration. The first 10–20 mL of filtrated solution were collected in a separate flask and filtrated again until no fine V_2O_5 was passing through the filter paper. The clear filtrate was collected in an argon flushed 1 L round bottom flask. After the filtration, the solution was distilled under argon atmosphere. First, the residual ^{n}BuOH was distilled away from the crude product mixture at normal pressure. Subsequently, the temperature was increased and the pressure was reduced to distil the vanadic acid ester from the crude product. A cold trap (196°C) was installed between the distillation and the Schlenk line. Distillation (145°C, 1 mbar) gave the product as yellow liquid (30.3 g, 14% based on vanadium). ^{1}H NMR ($CDCl_3$, 400 MHz) $\delta = 4.96$ (br. s, 6H), 1.78 (m, 6H), 1.55 (m, 6H), 0.96 (t, J = 7 Hz, 9H). ^{13}C NMR ($CDCl_3$, 100 MHz) $\delta = 82.4, 35.7, 19.0, 13.9$. ^{51}V NMR ($CDCl_3$, 105 MHz) $\delta = -595$.

Preparation of [V_6O_7(O^nPr)$_{12}$] (3).—In the glove box, VO(O^nPr)$_3$ (0.300 g, 1.2 mmol), [^{n}Bu$_4$N][BH$_4$] (0.132 g, 0.5 mmol), and *n*-propanol (10 mL) were charged in a 25 mL Teflon-lined autoclave. The reactor was sealed, removed from the glove box and placed in an oven where the mixture was heated to 125°C for 24 h. The autoclave was removed from the oven and cooled to room temperature over three hours. The subsequent workup was completed in ambient atmosphere. The resulting deep red solution was left exposed to air for one hour, during which the color slowly turned the distinct green of a mixed-valent, hexavanadate cluster. The crude product was chromatographed on a silica column (*n*-propanol), and the first, light green fraction collected. The solvent was evaporated under reduced pressure, and the product was extracted with acetonitrile, then dried under reduced pressure to give the product, **3**, as a sticky, green solid (0.125 g, 0.1 mmol, 54%). Crystals suitable for X-ray diffraction were grown from slow evaporation of *n*-propanol at room temperature. ^{1}H NMR (500 MHz, MeCN-d$_3$): $\delta = 26.8$ (br). FT-IR (ATR, cm^{-1}) 1036, 989 (O_b−R), 968 (V = O_t). UV−Vis (CH_3CN) [ε (M^{-1} cm^{-1})]: 384 nm (4.70×10^3), 1000 nm (1.24×10^3). ESI-MS(+): *m/z* 1127 [V_6O_7(O^nPr)$_{12}$]. Elemental analysis: Calculated (%) for (MW = 1127 g/mol): C, 38.38; H, 7.51%. Found: C, 38.40; H, 7.53%.

Preparation of [V_6O_7(O^nBu)$_{12}$] (4).—In the glove box, VO(O^nBu)$_3$ (0.300 g, 1.0 mmol), [^{n}Bu$_4$N][BH$_4$] (0.090 g, 0.4 mmol), and *n*-butanol (10 mL) were charged in a 25 mL Teflon-lined autoclave. The reactor was sealed, removed from the glove box and placed in an oven where the mixture was heated to 125°C for 24 h. After this time, the autoclave was removed from the oven and set to stand at room temperature for three hours. The subsequent workup was completed under an ambient atmosphere. The resulting deep red solution was left exposed to air for one hour, during which time the color of the solution slowly turned green. The crude product was then chromatographed on a silica column (*n*-butanol), and the first, light green fraction was collected. The solvent was evaporated under reduced pressure, and the product was extracted with acetonitrile, then dried *in vaccuo* to give the desired product, **4**, as a dark green oil (0.099 g, 0.1 mmol, 44%). ^{1}H NMR (500 MHz, MeCN-d$_3$): $\delta = 26.6$ (br). FT-IR (ATR, cm^{-1}) 1043, 1026, 1007 (O_b−R), 972 (V = O_t). UV−Vis (CH_3CN) [ε (M^{-1} cm^{-1})]: 384 nm (5.93×10^3), 1000 nm (1.11×10^3). ESI-MS(+): *m/z* 1295 (V_6O_7(O^nBu)$_{12}$), 1253 (V_6O_7 (OMe)(O^nBu)$_{11}$). Calculated (%) for combined MW = 1285 g/mol ([V_6O_7(OCH$_3$)$_x$(OC$_4$H$_9$)$_{1-x}$], where x = 1 for 25% and x = 0 for 75%): C, 44.18; H, 8.36%. Found: C, 44.178; H, 8.529%).

Solubility measurements.—The molar absorption coefficient of each species was determined using five stock solutions, serially diluted to absorbances between 0.1 and 1.0 in accordance with the Beer-Lambert relationship. Saturated solutions were prepared in triplicate by the sequential addition of solid into acetonitrile (3 mL) with stirring until a suspension was formed. The suspensions were stirred overnight, and then allowed to settle for at least 1 h, after which time the solutions were filtered through glass wool to remove any undissolved material. An aliquot of each solution was diluted in acetonitrile

Figure 1. General synthetic scheme for the synthesis of POV-alkoxide clusters.

and the UV-Vis spectra recorded to determine the maximum solubility of each species.

Bulk electrolysis and stability studies.—Bulk electrolysis experiments were performed with stirred solutions in an H-cell with a glass frit separator (Porosity = 10–16 μm, Pine Research, USA) using a Bio-Logic VMP3 potentiostat/galvanostat. An active species concentration of 1 mM was used. Each working electrode compartment contained 15 mL of the active species solution with 0.1 M $TBAPF_6$ in CH_3CN, and each counter electrode compartment had 15 mL of 0.1 M $TBAPF_6$ in CH_3CN. A Pt mesh working electrode and a Pt wire counter electrode were used. Bulk electrolysis experiments were carried out using the chronoamperometry techniques available in the Bio-Logic EC lab software suite at constant potentials, selected based on CV experiments. All experiments were conducted at room temperature inside a nitrogen-filled glove box (MBraun, USA).

Cyclic voltammetry (CV).—CV data were collected using a Bio-Logic SP 300 potentiostat/galvanostat and the EC-Lab software suite. Cyclic voltammograms were recorded using a 5.5 mm diameter platinum fixed-disk PEEK shroud working electrode (PINE Research, Durham, NC), a Pt wire auxiliary electrode (CH Instruments, USA), and a Ag/Ag^+ non-aqueous reference electrode with 0.01 M $AgNO_3$ in 0.1 M $TBAPF_6$ in CH_3CN (BASi, USA). All measurements were obtained at room temperature. Prior to data collection all solutions were bubbled with nitrogen. Cyclic voltammograms were iR compensated at 85% with impedance taken at 100 kHz using the ZIR tool included within the EC-Lab software. All CV experiments were repeated three times.

Rotating disk electrode (RDE) experiments.—A Pine MSR rotator (PINE Research, Durham, NC) was used for RDE experiments. The exact same configuration as the CV experiments were used to avoid any changes due to physically different electrodes. The working electrode was rotated at values spanning from 300 RPM to 2500 RPM, while the voltage was linearly swept from 0 V vs. OCV to 1.5 V and −0.55 V vs. Ag/Ag^+ non-aqueous reference electrode, at 5 mV/s for oxidation and reduction, respectively. All RDE experiments were repeated three times. The Koutecky-Levich analysis technique included within the EC-Lab software were used to calculate the heterogeneous electron transfer rate constants of each redox couple.

Results and Discussion

Synthesis and characterization.—The general synthetic scheme for the synthesis of POV-alkoxide clusters is shown in Figure 1. The syntheses of the propyl and butyl clusters, $[V_6O_7(O^nPr)_{12}]$ (**3**) and $[V_6O_7(O^nBu)_{12}]$ (**4**) were accomplished using protocols derived from those established for $[V_6O_7(OEt)_{12}]$ (**2**). To generate each of the longer chain alkyl complexes, a vanadium(V) ester precursor ($VO(OR)_3$; R = C_3H_7, C_4H_9) was dissolved in the respective alcohol (ROH; R = C_3H_7, C_4H_9), and subjected to solvothermal conditions along with the external reductant, tetrabutylammonium borohydride $[^nBu_4N][BH_4]$. While in the case of the formation of the methoxide-substituted POV-alkoxide cluster, $[V_6O_7(OMe)_{12}]$ (**1**), the reducing nature of methanol facilitates formation of the mixed-valent Linqvist ion, in the absence of external reductant, the longer chain alkyl complexes **2**, **3**, and **4** all require $[^nBu_4N][BH_4]$, in increasing proportions corresponding to the increasing alkyl chain length. Following the 24 hour solvothermal reaction, the reaction mixtures of **3** and **4** are exposed to air, whereupon they undergo a color change from red to green over the course of thirty minutes. Once the green color is observed, characterization by electrospray ionization mass spectrometry (ESI-MS) reveals *m/z* peaks corresponding to those predicted for **3** and **4** (*m/z* = 1127 and 1295, respectively). Following purification via chromatography on silica, complexes **3** and **4** are obtained in their neutral state, with oxidation state distributions of vanadyl ions matching that of the neutral clusters of **1** and **2** ($V^{IV}_4V^V_2$). Characterization via ^1H NMR, infrared, and electron absorption spectroscopies reveal the expected features for a delocalized, mixed valent vanadium core (Figure 2). In the case of **3**, we were able to grow crystals suitable for X-ray analysis, allowing for the unambigious confirmation of its structure (Figure 3).

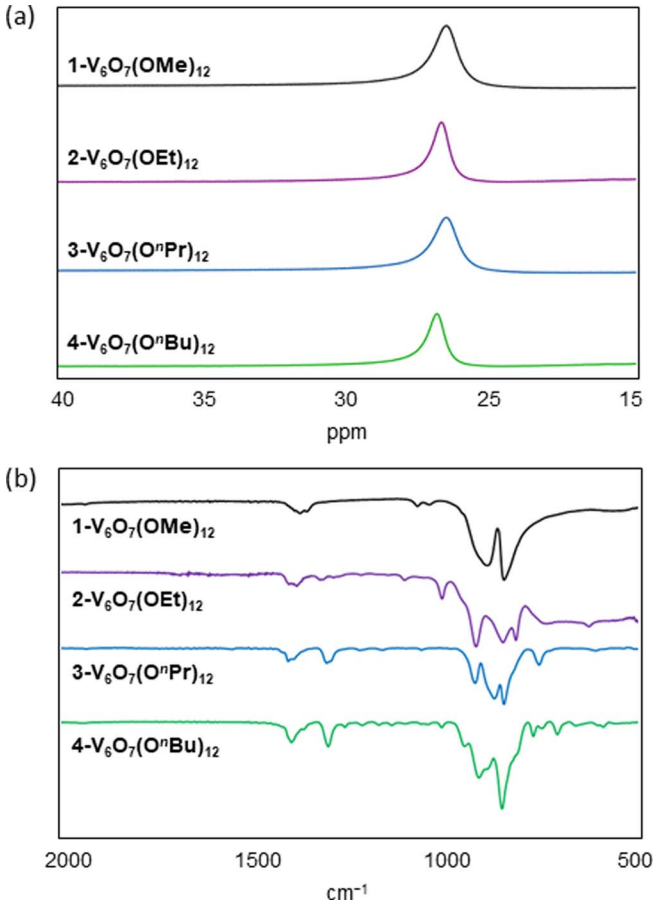

Figure 2. The NMR spectra (a), and the IR spectra (b) obtained for each species.

Interestingly, although the ESI-MS of **3** shows only a single peak corresponding to the fully propyl-bridged cluster, $[V_6O_7(O^nPr)_{12}]$ (*m/z* = 1127), in the spectrogram of **4**, a second peak is observed in addition to the expected peak of the fully butyl-bridged cluster $[V_6O_7(O^nBu)_{12}]$ (*m/z* = 1295). This second peak, with *m/z* = 1253, has a relative intensity of ~30% that of the primary peak, and corresponds to the substitution of a single bridging-butoxide for a bridging-methoxide moiety, to generate $[V_6O_7(OCH_3)(OC_4H_9)_{11}]$. Although clearly observable via ESI-MS, this "impurity", appears to have no impact on the redox profile of the cluster, and is not observed in the ^1H NMR and IR spectra of **4**. It is, however, detectable by elemental analysis, which reveals carbon and hydrogen percentages that reflect one quarter of the clusters having a single bridging-butoxide substituted for a bridging-methoxide ($[V_6O_7(OCH_3)_x(OC_4H_9)_{1-x}]$, where x = 1 for 25% and x = 0 for 75%; calculated (%) for combined MW = 1285 g/mol: C, 44.18; H, 8.36%. Found: C, 44.178; H, 8.529%). Attempts to avoid this impurity via modifications to the synthetic routes,

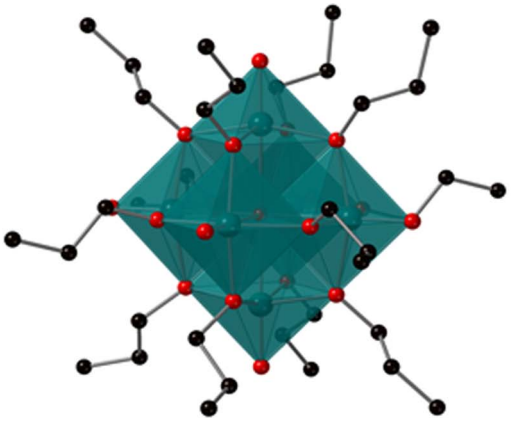

Compound	3-$V_6O_7(O^nPr)_{12}$
CCDC	1874261
Empirical formula	$C_{36}H_{84}O_{19}V_6$
Formula weight	1126.67
Temperature / K	232.99(11) K
Wavelength / Å	1.54184 Å
Crystal system	trigonal
Space group	P-3_m
Unit cell dimensions	a = 19.6327(2) Å b = 19.6327(2) Å c = 11.6206(2) Å α = 90° β = 90° Υ = 120°
Volume / Å^3	3878.99(10) Å^3
Z	3
Reflections collected	13601
Independent reflections	1000
Completeness (theta)	100.0 % (74.504°)
Goodness-of-fit on F2	1.171
Final R indices [I>2sigma(I)]	R1 = 0.0381
Largest diff. peak and hole	0.212 and -0.292 Å^{-3}

Figure 3. X-ray crystal structure of $[V_6O_7(O^nPr)_{12}]$.

or to separate it via chromatography, were unsuccessful. However, owing to its apparent lack of impact on the electrochemical profile of **4**, we continued our analysis.

Solubility measurements.—The solubilities of complexes **3** and **4** were measured in acetonitrile in the presence of 0.1 M $TBAPF_6$, in order to mimic the conditions of a working, naRFB cell. The solubilities were measured to be 0.097 M and 0.297 M for **3** and **4**, respectively. The limited solubility of **3** is contrary to our original hypothesis that the increased alkyl chain length would promote solubility in organic solvent. Instead, we find that while this propoxide-bridged cluster has increased solubility over the ethoxide-bridged **2** (0.052 M), its solubility is significantly less than that of the methoxide-bridged cluster, **1** (0.205 M). Interestingly, the butyl-bridged complex **4** has significantly improved solubility over all other alkyl derivatives, and is notably the only complex to be an oil at room temperature.

The least soluble component of an electrolyte couple in an RFB determines the upper limit of concentration for calculations of energy density. For species that cycle between multiple charge states, it is important that no precipitation occurs during bulk electrolysis. We did not observe any aggregation or precipitation during bulk electrolysis experiments at the solubility limit of each neutral cluster, indicating that the other charge states are equal or more soluble than this limiting value. Thus, we took the concentration of the neutral cluster as the parameter for calculations of energy density. Using these solubility values we calculated the specific energy densities to be $[V_6O_7(OMe)_{12}]$ = 5.14 kJ/L, $[V_6O_7(OEt)_{12}]$ = 8.38 kJ/L, $[V_6O_7(O^nPr)_{12}]$ = 16.38 kJ/L, and $[V_6O_7(O^nBu)_{12}]$ = 52.44 kJ/L.

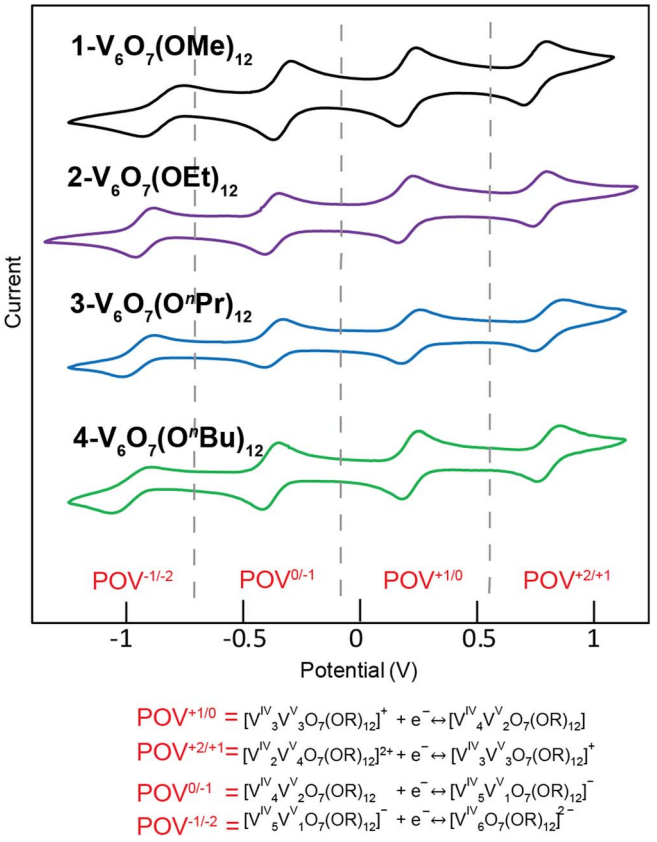

Figure 4. CV profiles obtained for POV-alkoxide clusters at a Pt working electrode using 1 mM of active species in 0.1 M $TBAPF_6$ in CH_3CN: scan rate = 100 mV/s.

Bulk electrolysis and stability studies.—The CVs for all four POV-alkoxide clusters are shown in Figure 4. The electrochemical stability of complexes **1** and **2** were previously reported.[23] The electrochemical stability of complexes **3** and **4** was assessed using bulk electrolysis in conjunction with CV monitoring of the solutions. Bulk reduction and oxidation of solutions of **3** and **4** at −1.1 and +1.0 V vs Ag/Ag^+, respectively, yielded no change in the redox profiles of the solution, apart from the expected shift in open circuit potential (Figure 5). The open circuit potential (OCP) of the propoxide cluster shifted from the initial value of 0.12 V vs. Ag/Ag^+ to 0.97 V vs. Ag/Ag^+ upon oxidation and −0.99 V vs. Ag/Ag^+ upon reduction. For the butoxide cluster the OCP value changed from 0.06 V vs. Ag/Ag^+ to 0.93 V vs. Ag/Ag^+ and −1.07 V vs. Ag/Ag^+ upon oxidation and reduction, respectively. These OCPs are beyond the $E_{1/2}$ values for the corresponding redox events, as expected for successful electrolysis. The electrolyzed solutions were subsequently monitored for both decomposition and self-discharge using CV and open circuit potential measurements over the course of one week, confirming the stability of both **3** and **4** in their charged states. The observed stability of the propoxide- and butoxide-bridged polyoxovanadate clusters is consistent with our previously noted trend that increasing the length

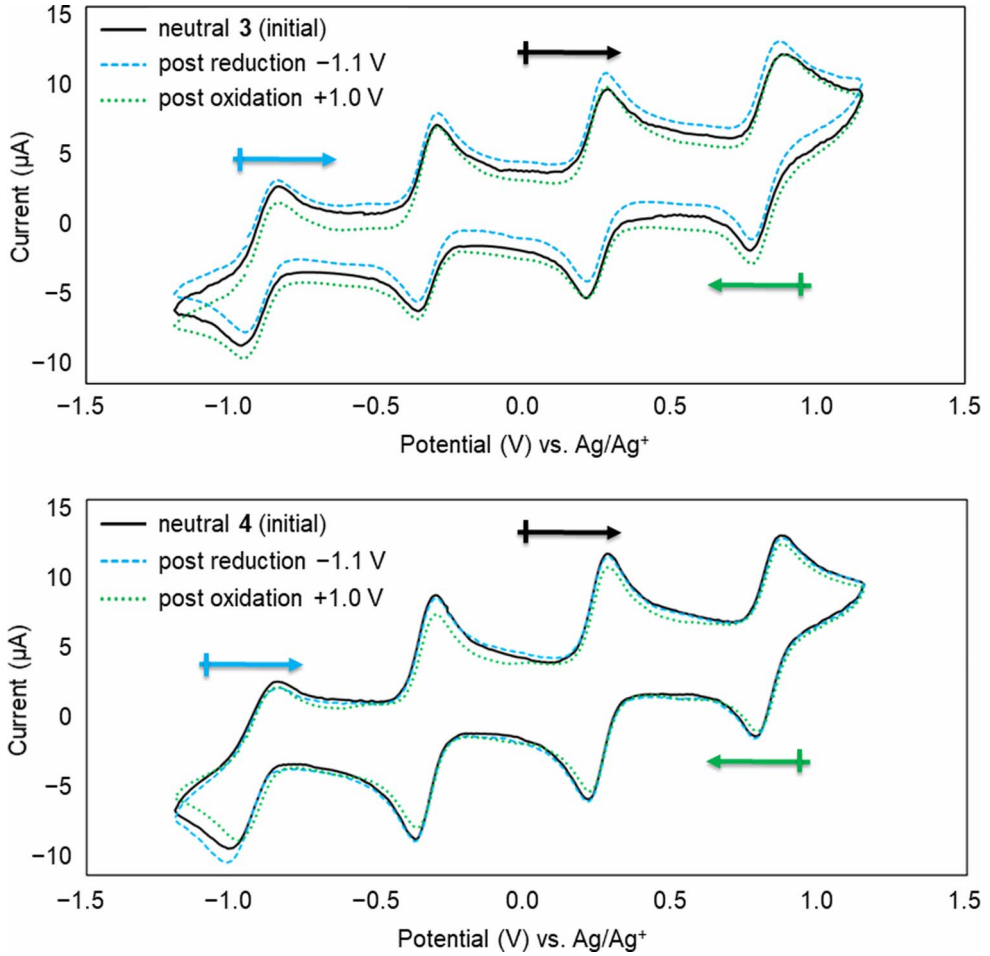

Figure 5. Bulk electrolysis and stability monitoring of complex 3 and 4 via cyclic voltammetry. Arrows indicate sweep direction and open circuit potential.

of the bridging alkyl chain in the POV-alkoxide clusters results in the electrochemically stable complexes over all four redox events.[23]

Transport and electron transfer kinetics of homoleptic POV-alkoxide clusters.—*Diffusion coefficients (D_0) of the homoleptic POV-alkoxide clusters.*—The D_0 values of all four POV-alkoxide clusters were calculated using the Randles-Sevcik method. A scan-rate-dependent CV study was performed, with POV-alkoxide clusters **1–4** in 0.1 M $TBAPF_6$ in CH_3CN. Scan rates ranging from 25 mV/s to 1500 mV/s were used. The first oxidation (anodic) and first reduction (cathodic) peaks of the neutral clusters were used to calculate the average D_0 values. All redox couples in the study appeared quasi-reversible, as we see both anodic and cathodic waves, yet the peak separations (ΔE_p) were all > 59 mV.[8,42,43] Figure 6a shows a scan rate dependent CV, obtained for the first oxidation and reduction redox couples of complex **1**. Similar CV profiles were obtained for **2–4**. Linear relationships were observed between peak currents and the square root of scan rate for all redox couples in the study. In Figure 6b, peak current versus the square root of scan rate plots for the first anodic and cathodic peaks of the methoxide cluster are shown. The observed linearity indicates diffusion controlled redox reactions.[9,10,44] For a reversible redox couple, peak current, i_p is given by the following equation;

$$i_p = 2.69 \times 10^5 n^{3/2} A\, c D_0{}^{1/2} \nu^{1/2} \quad [2]$$

For an irreversible redox couple, the peak current, i_p is given by the following equation

$$i_p = 2.99 \times 10^5 n^{3/2} \alpha^{1/2} A\, c D_0{}^{1/2} \nu^{1/2} \quad [3]$$

In Eqs. 2 and 3, n is the number of electrons transferred, α is the charge transfer coefficient ($\alpha \sim 0.5$), A is the electrode area (0.2376 cm^2 for the Pt working electrode), c is the bulk concentration of the active species, D_0 is the diffusion coefficient of the active species and ν is

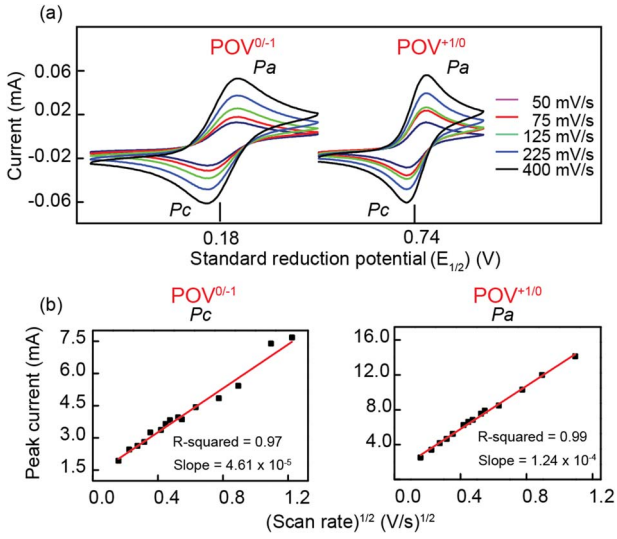

Figure 6. Scan rate dependent CV profiles for the first oxidation and first reduction redox couples of POV-methoxide cluster (a) and the peak current versus square root of scan rate plots for redox couples of complex 01 (b).

Table I. Diffusion coefficients of neutral POV-alkoxide clusters calculated using the Randles-Sevcik method.

Species	Reversible Randles-Sevcik equation (10^{-5} cm^2/s)	Irreversible Randles-Sevcik equation (10^{-5} cm^2/s)
$V_6O_7(OMe)_{12}$	0.17	0.18
$V_6O_7(OEt)_{12}$	0.15	0.24
$V_6O_7(O^nPr)_{12}$	0.15	0.25
$V_6O_7(O^nBu)_{12}$	1.39	2.25

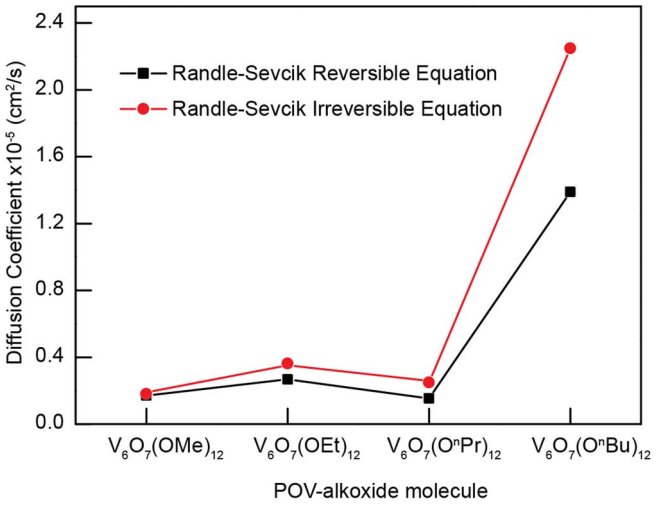

Figure 7. Plots of diffusion coefficients calculated using the reversible and irreversible Randles-Sevcik equations for the neutral POV-alkoxide clusters.

the scan rate. Since there is no equation to explicitly calculate the diffusion coefficients for a quasi-reversible reaction, we report the values obtained from the reversible and irreversible treatments for upper and lower limits of D_0. The estimated D_0 values obtained for the neutral POV-alkoxide clusters using the Randles-Sevcik method are shown in Table I.

As shown in Figure 7, no significant trend was observed between D_0 and the length of the alkyl chain of the alkoxide ligands. Following the Stokes-Einstein relationship, we expect $[V_6O_7(O^nBu)_{12}]$ to have a smaller D_0, as it is the largest amongst the four POV-alkoxide clusters studied.[45] Despite this expectation, the butoxide cluster demonstrated higher values compared to other three clusters, indicative that between C1 and C4 alkyl chains, the size of the alkoxide ligand is not a critical determinant of diffusion behavior. Similar observations were also made with chromium and vanadium acetylacetonate complexes, where changing the ligand chain length resulted in only trivial changes to the diffusion coefficients and electron transfer rate constants.[25,26]

A similar correlation between D_0 values and charge state was observed for the ethoxide cluster. We calculated the D_0 values of chemically and electrochemically isolated redox states of the POV-ethoxide. Both samples resulted in D_0 values that are within the same order of magnitude for +1, +2, −1, and −2 states as reported in Table II. The D_0 values increase as the overall charge of the clusters

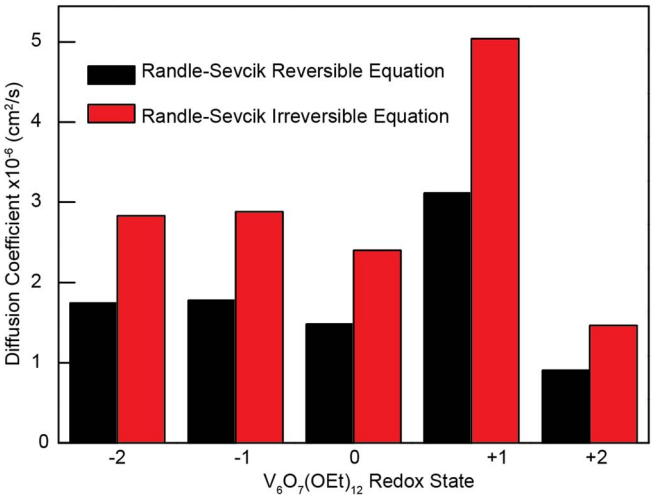

Figure 8. Diffusion coefficients of POV-ethoxide cluster at varied redox states calculated using Randles-Sevcik method.

became more negative (Figure 8), indicating that the anionic species displayed better mass transport. The D_0 of the +1 charged complex was the highest amongst all relevant charge states suggesting that the hydrodynamic radius is smallest at this state.

Heterogeneous electron transfer rate constants (k_0) of homoleptic POV-alkoxide clusters.—The k_0 values were determined using three different methods, (1) the Nicholson,[46] (2) the Kochi-Klinger,[36] and (3) the Koutecky-Levich.[37] The Nicholson and Kochi-Klinger methods all use steady-state models for the calculation of electrode reaction rates using CV data obtained at different scan rates and are based on peak-to-peak separation (ΔE_p). The Nicholson method is frequently used to estimate k_0 by relating ΔE_p with a dimensionless kinetic parameter (ψ). The dimensionless parameter (ψ) is obtained by introducing the ΔE_p values to the working curve described by Nicholson and Shain, and the heterogeneous electron transfer rate constant (k_0) for the redox reaction is calculated using the following equation:[46]

$$k_0 = \psi\left[\frac{\pi n F D_0 \nu}{RT}\right]^{1/2} \quad [4]$$

In Eq. 4, n is the number of electrons involved in the reaction, ν is the scan rate, F is the Faraday constant, ψ is the Nicholson dimensionless parameter, D_0 is the diffusion coefficient, R is the gas constant, and T is the temperature. The Kochi-Klinger method also depends on ΔE_p for estimating k_0. The following equation is used to calculate the k_0:[36]

$$k_0 = 2.18\left[\frac{\alpha n F D_0 \nu}{RT}\right]^{1/2} exp\left[\frac{-\alpha^2 n F\left(E_{pa} - E_{pc}\right)}{RT}\right] \quad [5]$$

Wherein α is the charge-transfer coefficient (~0.5) and E_{pa} and E_{pc} are the anodic and cathodic peak current potentials.

We also used RDE voltammetry as a third method for determining k_0. RDE experiments were carried out over a range of rotation rates from 300 rpm to 2500 rpm. Figure 9a shows the LSV

Table II. Diffusion coefficients calculated for all relevant redox states of the POV-ethoxide cluster.

	Reversible Randles-Sevcik equation (10^{-6} cm^2/s)		Irreversible Randles-Sevcik equation (10^{-6} cm^2/s)	
Redox State	Electrochemically isolated species	Chemcially isolated species	Electrochemically isolated species	Chemcially isolated species
−2	1.5	1.7	2.4	2.8
−1	3.3	1.8	5.3	2.9
+1	3.2	3.1	5.2	5.0
+2	0.7	0.9	1.2	1.5

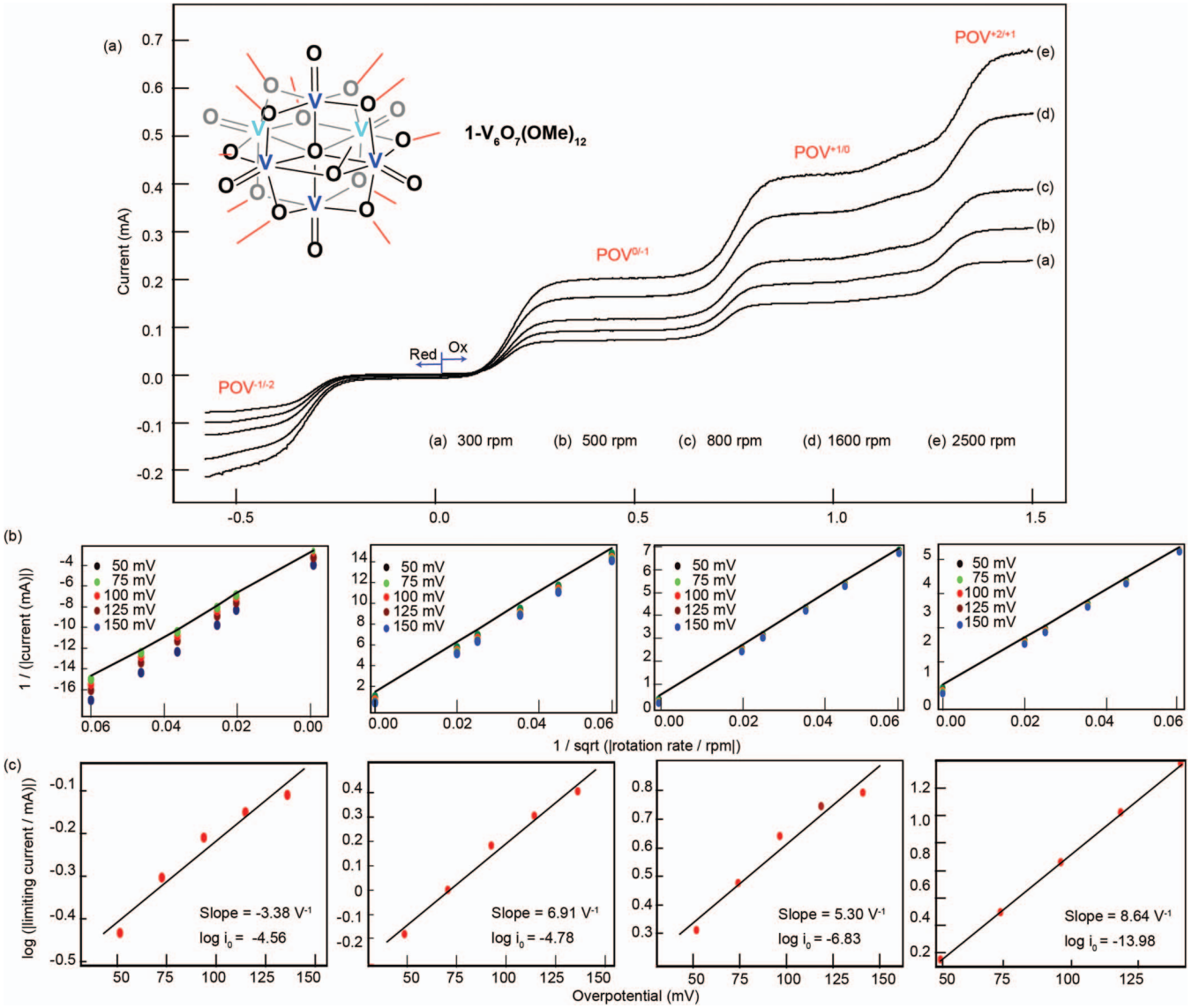

Figure 9. RDE data for complex 01(a), Koutecky-Levich plots (b), and Tafel plots (c) for redox couples of POV-methoxide cluster.

profiles obtained in RDE experiments for **1**. Similar LSV data were observed with the other three alkoxide clusters as well. The current responses at varied overpotentials were used to construct Koutecky–Levich plots, which were used to determine mass-transfer-independent kinetic currents i_k for redox reactions. These i_k values were subsequently fit to the Butler-Volmer equation via Tafel plots. Using the Tafel equation shown below, the rate constants were calculated.

$$log\ i_k = \log(nFcAk_0) + \frac{nF\alpha\eta}{2.303\ RT} \quad [6]$$

In Eq. 6, n is the number of electrons, α is the transfer coefficient, R is the gas constant, T is temperature, k_0 is the standard kinetic rate constant, and η is the over potential. The Koutecky–Levich plots and the corresponding Tafel plots for the four redox couples of methoxide cluster are shown in Figure 9. The average value of three trials for the electron transfer rate constants are shown in Table III. The estimated k_0 values for all redox couples are in the range of 10^{-2} cm/s - 10^{-3} cm/s, values that are competitive with existing naRFB charge-carriers.[47]

The molecular structure of redox active species is expected to affect electron transfer kinetics in both outer-sphere and inner-sphere microscopic models of electron transfer. The Marcus theory of electron transfer further states that the probability of electron transfer events decreases with increasing distance between the donor and acceptor. It is therefore reasonable to expect changes in electron transfer rate constants in POV-alkoxide clusters of varying side chain sizes. The results show that regardless of the length of the alkyl chains of the alkoxide ligands, these clusters all show fast electron transfer kinetics as estimated from four different electroanalytical methods and with no clear trends, i.e. the longer the chain, the slower the electron transfer (Figure 10). We therefore conclude that the reorganization energy (λ) of POV-alkoxide clusters does not vary with the size between C1 and C4 alkyl lengths, thus there is a minimal impact on the overall electron transfer kinetics and transport phenomena. This is a promising result given that a common strategy to increase solubility is to modify pendant organic functionality and we have also established that such modifications can increase stability, thereby enabling multi-electron transfer. We expect to further explore the electrochemical and physicochemical behaviors of POV-alkoxide clusters in other organic solvents and evaluate the performance in varied membrane separators toward identifying more compatible active species-membrane-solvent composites in the near future.

Table III. Heterogeneous electron transfer rate constants from CV and RDE methods.

Species and Redox Couples		Heterogeneous electron transfer rate constant (cm/s)		
		RDE	*CV*	
		Koutecky-Levich ($\times 10^{-2}$)	Nicholson ($\times 10^{-3}$)	Kochi ($\times 10^{-3}$)
$V_6O_7(OMe)_{12}$	**$POV^{1+/0}$**	7.67 ± 0.62	20.00 ± 2.71	4.10 ± 0.15
	$POV^{2+/1+}$	7.30 ± 0.68	14.00 ± 6.44	3.50 ± 0.32
	$POV^{0/1-}$	2.03 ± 0.03	0.93 ± 0.01	0.81 ± 0.02
	$POV^{1-/2-}$	0.86 ± 0.16	17.00 ± 1.28	3.10 ± 0.05
$V_6O_7(OEt)_{12}$	**$POV^{1+/0}$**	7.45 ± 0.09	125.00 ± 12.45	7.44 ± 0.63
	$POV^{2+/1+}$	5.06 ± 1.25	209.00 ± 56.32	7.39 ± 0.43
	$POV^{0/1-}$	1.48 ± 0.33	8.46 ± 6.24	7.27 ± 0.43
	$POV^{1-/2-}$	0.68 ± 0.24	13.30 ± 1.27	2.92 ± 1.38
$V_6O_7(O^nPr)_{12}$	**$POV^{1+/0}$**	1.05 ± 0.01	25.00 ± 1.66	4.60 ± 0.08
	$POV^{2+/1+}$	1.39 ± 0.04	68.00 ± 1.53	7.60 ± 0.75
	$POV^{0/1-}$	4.69 ± 0.01	21.00 ± 0.78	3.20 ± 0.04
	$POV^{1-/2-}$	0.24 ± 0.00	0.56 ± 0.06	0.52 ± 0.02
$V_6O_7(O^nBu)_{12}$	**$POV^{1+/0}$**	0.77 ± 0.11	52.00 ± 9.77	9.50 ± 0.97
	$POV^{2+/1+}$	2.94 ± 0.29	69.50 ± 9.85	11.60 ± 2.05
	$POV^{0/1-}$	1.23 ± 0.08	13.70 ± 0.79	8.30 ± 0.08

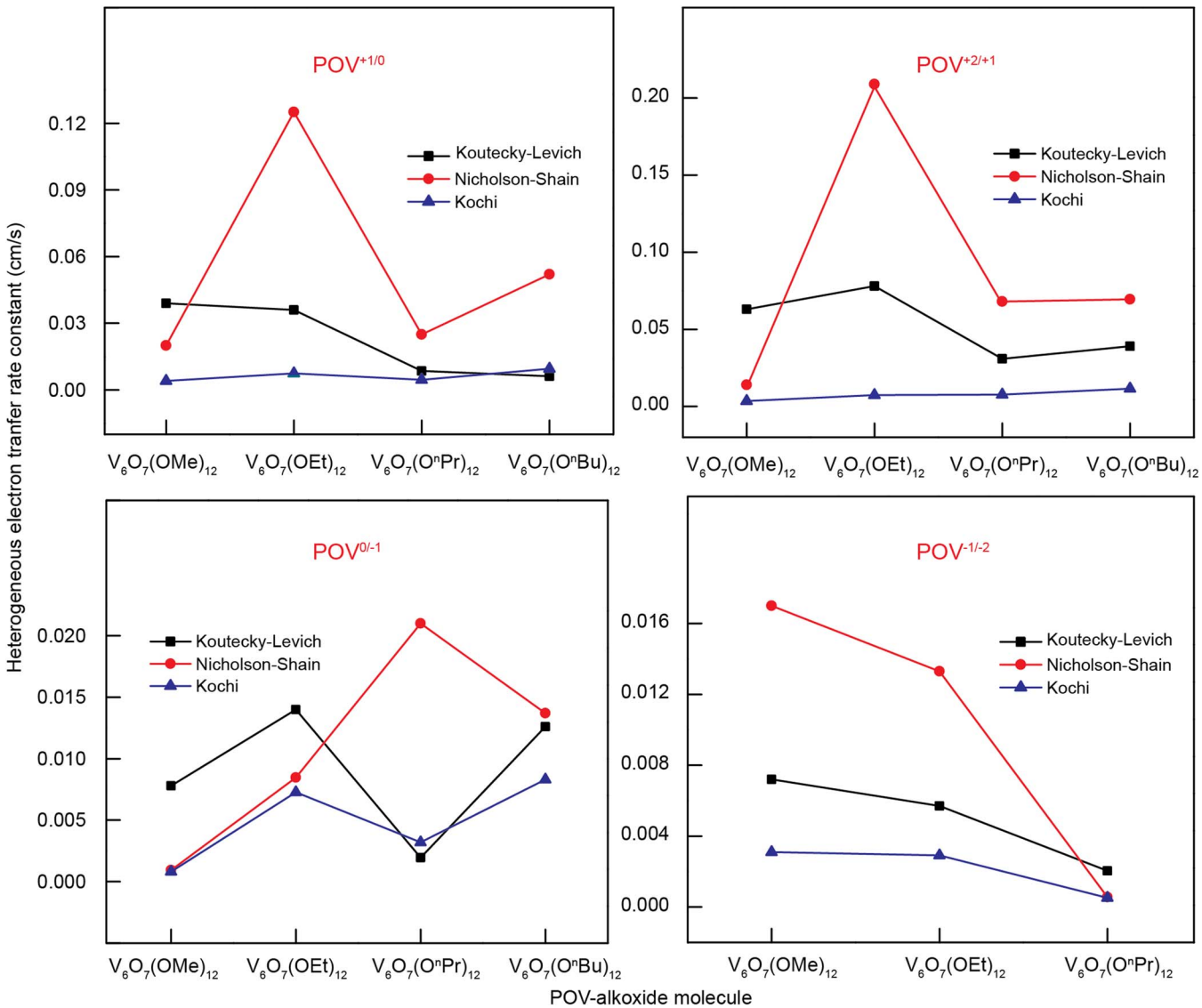

Figure 10. Plots of heterogeneous electron transfer rate constants of each redox couple versus the chain length of POV-alkoxide clusters.

Summary

In this work, we evaluated electrochemical and physicochemical properties of a series of POV-alkoxide clusters, toward developing superior charge-carriers for naRFBs. We place an emphasis on evaluating whether ligand substitution has a deleterious effect on redox behavior. The bridging alkoxide ligands in our POV clusters were modified to obtain $[V_6O_7(OMe)_{12}]$, $[V_6O_7(OEt)_{12}$, $[V_6O_7(O^nPr)_{12}]$, and $[V_6O_7(O^nBu)_{12}]$. The butoxide cluster has the highest solubility of ∼0.3 M amongst the four clusters studied. At these cell voltages, solubilities of ∼3 M are needed to match state-of-the-art energy densities in all-vanadium aqueous RFBs. Alternative ligand substitutions and heterometallic cores offer promising directions to improve both cell voltage and solubility further, in an effort to raise energy densities even higher. The ethoxide, propoxide, and butoxide clusters all demonstrate long term stabilities as shown by bulk electrolysis and CV experiments. CV data enabled estimation of diffusion coefficients by using peak current responses at different scan rates (the Randles-Sevcik method). The heterogeneous electron transfer rate constants were also determined in multiple ways: (a) the Nicholson and (b) the Kochi-Klinger, using the peak separation potentials at varied scan rates from CV experiments; and (c) the Koutecky-Levich analysis using current extrapolated from RDE liner sweep voltammetry data in the kinetically controlled region. These electrochemical studies reveal that the metal-alkoxide clusters uniformly exhibit fast electron transfer kinetics in the regimes of 10^{-2} - 10^{-3} cm/s. In addition, we observe no trend correlating the diffusion coefficient of a given POV-alkoxide and the size of the bridging ligands. Due to the diffusion controlled nature of all redox reactions involved and the fast electron transfer kinetics, there will be minimal charge-transfer and mass transport losses, regardless of alkyl chain length in EES devices that use POV-alkoxide clusters as charge-carriers. Hence, it is concluded that the improvements in solubility and long-term stability do not cost the inherent fast electron transfer properties of the bridging ligand modified POV-alkoxide clusters. As a result, modifying the alkyl chains of alkoxide ligands is an effective vector for tuning physicochemical properties.

Acknowledgments

This research was supported by the University at Buffalo, SUNY (A.M.K., J.P.H., and T.R.C.) and the University of Rochester (L.E.V. and E.M.M.). L.E.V. also acknowledges the National Science Foundation for fellowship support (NSF-GRFP, DGE-1419118).

ORCID

Timothy R. Cook https://orcid.org/0000-0002-7668-8089

References

1. B. Dunn, H. Kamath, and J.-M. Tarascon, *Science*, **334**, 928 (2011).
2. S.-H. Shin, S.-H. Yun, and S.-H. Moon, *RSC Advances*, **3**, 9095 (2013).
3. R. Darling, K. Gallagher, W. Xie, L. Su, and F. Brushett, *Journal of The Electrochemical Society*, **163**, A5029 (2016).
4. R. M. Darling, K. G. Gallagher, J. A. Kowalski, S. Ha, and F. R. Brushett, *Energy & Environmental Science*, **7**, 3459 (2014).
5. K. Gong, Q. Fang, S. Gu, S. F. Y. Li, and Y. Yan, *Energy & Environmental Science*, **8**, 3515 (2015).
6. M. H. Chakrabarti, R. A. W. Dryfe, and E. P. L. Roberts, *Electrochimica Acta*, **52**, 2189 (2007).
7. J. L. Barton, T. Carney, and F. R. Brushett, *Meeting Abstracts*, **MA2016-02**, 638 (2016).
8. Q. Liu, A. A. Shinkle, Y. Li, C. W. Monroe, L. T. Thompson, and A. E. S. Sleightholme, *Electrochemistry Communications*, **12**, 1634 (2010).
9. Q. Liu, A. E. S. Sleightholme, A. A. Shinkle, Y. Li, and L. T. Thompson, *Electrochemistry Communications*, **11**, 2312 (2009).
10. D. Zhang, H. Lan, and Y. Li, *Journal of Power Sources*, **217**, 199 (2012).
11. M. H. Chakrabarti, E. P. L. Roberts, C. Bae, and M. Saleem, *Energy Conversion and Management*, **52**, 2501 (2011).
12. A. M. Kosswattaarachchi, A. E. Friedman, and T. R. Cook, *ChemSusChem*, **9**, 3317 (2016).
13. A. Iordache, V. Delhorbe, M. Bardet, L. Dubois, T. Gutel, and L. Picard, *ACS Applied Materials & Interfaces*, **8**, 22762 (2016).
14. J. Winsberg, C. Stolze, S. Muench, F. Liedl, M. D. Hager, and U. S. Schubert, *ACS Energy Letters*, **1**, 976 (2016).
15. C. S. Sevov, R. E. M. Brooner, E. Chénard, R. S. Assary, J. S. Moore, J. Rodríguez-López, and M. S. Sanford, *Journal of the American Chemical Society*, **137**, 14465 (2015).
16. S. Zhang, X. Li, and D. Chu, *Electrochimica Acta*, **190**, 737 (2016).
17. X. Wei, W. Xu, J. Huang, L. Zhang, E. Walter, C. Lawrence , M. Vijayakumar, W. A. Henderson, T. Liu, L. Cosimbescu, B. Li, V. Sprenkle, and W. Wang, *Angewandte Chemie International Edition*, **54**, 8684 (2015).
18. F. R. Brushett, J. T. Vaughey, and A. N. Jansen, *Advanced Energy Materials*, **2**, 1390 (2012).
19. J. Winsberg, T. Hagemann, S. Muench, C. Friebe, B. Häupler, T. Janoschka, S. Morgenstern, M. D. Hager, and U. S. Schubert, *Chemistry of Materials*, **28**, 3401 (2016).
20. G. Nagarjuna, J. Hui, K. J. Cheng, T. Lichtenstein, M. Shen, J. S. Moore, and J. Rodríguez-López, *Journal of the American Chemical Society*, **136**, 16309 (2014).
21. S. H. Oh, C. W. Lee, D. H. Chun, J. D. Jeon, J. Shim, K. H. Shin, and J. H. Yang, *Journal of Materials Chemistry A*, **2**, 19994 (2014).
22. J. D. Milshtein, J. L. Barton, T. J. Carney, J. A. Kowalski, R. M. Darling, and F. R. Brushett, *Journal of the Electrochemical Society*, **164**, A2487 (2017).
23. L. E. VanGelder, A. M. Kosswattaarachchi, P. L. Forrestel, T. R. Cook, and E. M. Matson, *Chemical Science*, **9**, 1692 (2018).
24. A. P. Kaur, N. E. Holubowitch, S. Ergun, C. F. Elliott, and S. A. Odom, *Energy Technology*, **3**, 476 (2015).
25. P. J. Cabrera, X. Yang, J. A. Suttil, R. E. M. Brooner, L. T. Thompson, and M. S. Sanford, *Inorganic Chemistry*, **54**, 10214 (2015).
26. J. A. Suttil, J. F. Kucharyson, I. L. Escalante-Garcia, P. J. Cabrera, B. R. James, R. F. Savinell, M. S. Sanford, and L. T. Thompson, *Journal of Materials Chemistry A*, **3**, 7929 (2015).
27. P. J. Cappillino, H. D. Pratt, N. S. Hudak, N. C. Tomson, T. M. Anderson, and M. R. Anstey, *Advanced Energy Materials*, **4**, 1300566 (2014).
28. J. Winsberg, T. Hagemann, T. Janoschka, M. D. Hager, and U. S. Schubert, *Angewandte Chemie International Edition*, **56**, 686 (2017).
29. L. E. VanGelder and Ellen M. Matson, *Journal of Materials Chemistry A*, **6**, 13874 (2018).
30. L. E. VanGelder, B. E. Petel, O. Nachtigall, G. Martinez, W. W. Brennessel, and E. M. Matson, *ChemSusChem*, 0.
31. S. Tejal and M. James, *A Benchmarking Approach for Routine Determination of Flow Battery Kinetics* (2018).
32. J. D. Milshtein, K. M. Tenny, J. L. Barton, J. Drake, R. M. Darling, and F. R. Brushett, *Journal of The Electrochemical Society*, **164**, E3265 (2017).
33. A. Orita, M. G. Verde, M. Sakai, and Y. S. Meng, *Nature Communications*, **7**, 13230 (2016).
34. A. Sevcik, *Coll. Czech. Chem. Comm*, **13**, 349 (1948).
35. R. S. Nicholson, *Analytical Chemistry*, **37**, 1351 (1965).
36. R. J. Klingler and J. K. Kochi, *The Journal of Physical Chemistry*, **85**, 1731 (1981).
37. J. K. A. V. G. Levich, *Zhur. Fiz. Khim.*, **32**, 1565 (1958).
38. C. Daniel and H. Hartl, *Journal of the American Chemical Society*, **127**, 13978 (2005).
39. G. M. Sheldrick, *SHELXT-2014/5*.
40. G. M. Sheldrick, *Acta Crystallographica Section C*, **71**, 3.
41. W. Prandtl and L. Hess, *Zeitschrift für anorganische Chemie*, **82**, 103 (1913).
42. A. E. S. Sleightholme, A. A. Shinkle, Q. Liu, Y. Li, C. W. Monroe, and L. T. Thompson, *Journal of Power Sources*, **196**, 5742 (2011).
43. G. Denuault, M. Sosna, and K.-J. Williams, in *Handbook of Electrochemistry*, C. G. Zoski Editor, p. 431, Elsevier, Amsterdam (2007).
44. N. Aristov and A. Habekost, *World Journal of Chemical Education*, **3**, 115 (2015).
45. M. Iwahashi and Y. Kasahara, *Journal of Oleo Science*, **56**, 443 (2007).
46. R. S. Nicholson and I. Shain, *Analytical Chemistry*, **36**, 706 (1964).
47. Y. Ding, Y. Zhao, Y. Li, J. B. Goodenough, and G. Yu, *Energy & Environmental Science*, **10**, 491 (2017).